Rakenteiden Mekaniikka (Journal of Structural Mechanics)
Vol. 41, No 3, 2008, pp. 119-136

A parametric fracture mechanics study of the effect of a cold lap defect on fatigue strength

Mikko Heiskanen

Summary. Several finite element analyses were carried out to study the effect of local geometrical variation of weld on fatigue strength of non-load-carrying cruciform joints in as-welded condition under tensile loading. Cruciform joints can be found in many heavy industrial applications, such as in junctions of longitudinal and transverse stiffeners in welded plate girders of shipyard cranes and orthotropic plates of ships. The variables were toe radius, cold lap and flank angle. The fatigue assessment was carried out with linear-elastic fracture mechanics in plane strain and under mixed-mode $K_I - K_{II}$ conditions. The Paris crack growth law was used to predict the growth rate. An analytical model was developed and its accuracy was compared to the available experimental fatigue test results.

Key words: fatigue crack growth, finite element analysis, fracture mechanics, mixed mode fracture, welded joints

Nomenclature

a	Crack length of cold lap
A	Throat thickness
C	Fatigue crack growth coefficient
E	Young's modulus
K_i	Stress intensity factor of mode i (i=I, II)
$K_{I_{ieq}}$	Equivalent stress intensity factor
K_{th}	Threshold stress intensity factor
m	Fatigue crack growth exponent
N	Number of cycles
r	Toe radius
R	Stress ratio
T	Plate thickness
β	Flank angle
Δ	Range in cyclic loading
$\Delta\theta_c$	Crack kink angle
ν	Poisson's ratio
σ	Normal stress
σ_y	Yield stress
BC	Boundary condition
FAT	Fatigue strength at $2 \cdot 10^6$ cycles with 95 % survival probability
FEA	Finite element analysis
IIW	International Institute of Welding

LEFM Linear-elastic fracture mechanics
LUT Lappeenranta University of Technology
MAG Metal Active Gas
SCF Stress concentration factor
SIF Stress intensity factor
S-N Stress-life curve

Introduction

It is well documented that welds are the weakest part of a fatigue-loaded structure due to local weld geometry and different types of weld imperfections which strongly affect on the fatigue strength. The local geometry affects on the local stress concentrations of a structure and the welding process can create crack-like defects, such as cold laps and undercuts, which during cyclic loading may lead to a large scatter in fatigue life. The conventional fatigue design rules for welded joints, which are based on the S-N curves, only partially consider weld defects what can initiate during fabrication. Usually, the S-N curves are based on the laboratory tests of welds with "normal" quality, even though, what is a normal quality is not always clearly specified. There is a demand for better understanding of the influence of macro-geometrical effects, structural discontinuities and weld defects that produce a high local stress.

Typical types of weld defects, what can be found on cruciform joints [1], are crack at the weld toe, crack at the root, interbead crack and cold lap and are usually the consequences of improper fabrication. Cold lap, Figure 1, is a weld defect, where the weld filler material has not properly fused with the base metal or the previous welds pass material [2]. The arc has not melted the base metal sufficiently and has caused a slightly molten puddle to flow into the base material without bonding. Numerous test programs have demonstrated the detrimental effect of cold laps and individual analysis results have shown influence of fatigue cracks growing from cold lap defects. An investigation covered by Lopez and Korsgen [3], proved that 80 % of all discovered weld defects in MAG (Metal Active Gas) welds are cold laps. The range of a typical cold lap size is between 0.01 – 0.14 mm. Moreover, there seems to be an obvious connection between high speed welding and the occurrence frequency of cold laps [4].

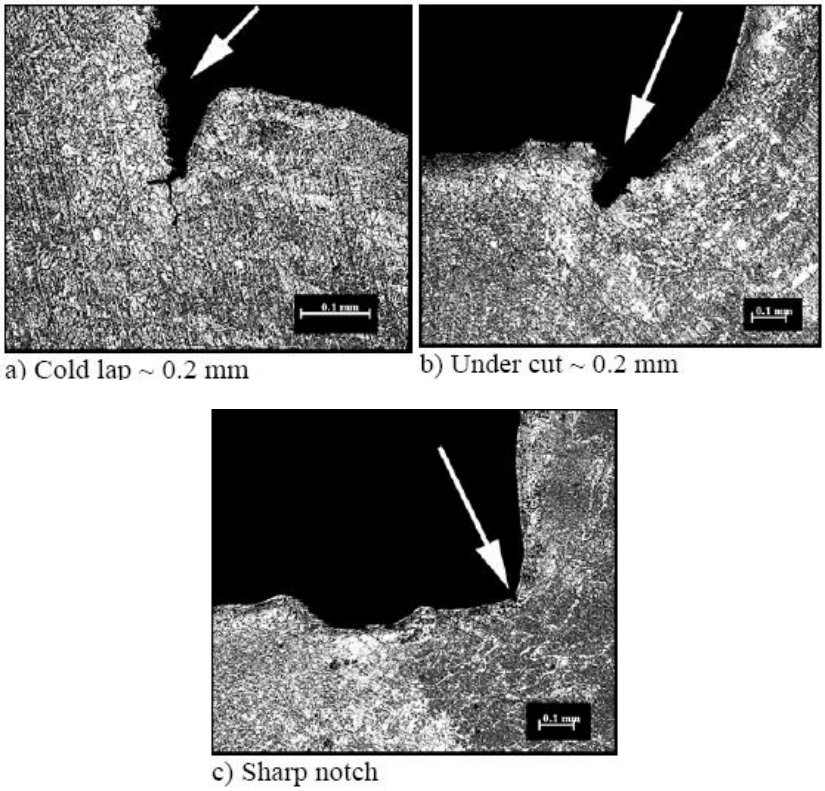

Figure 1. Typical crack-like defects on welded structures [5].

The objective of this work was to study the influence of cold laps on the fatigue strength of non-load-carrying fillet welded cruciform joints in as-welded condition under cyclic tensile loading. This was carried out with linear-elastic fracture mechanics (LEFM) in plain strain. The variables were cold lap size, toe radius and flank angle and the parametrical interdependence were analyzed with 90 different 2D finite element (FE) models and non-linear regression analysis. As a result of this study, an analytical model was developed and its validitation was verified with the comparison to experimental test results.

Fracture mechanics analysis

Stress intensity factor calculation

The opening mode and the sliding mode stress intensity factors K_I and K_{II} were calculated with FE crack growth simulation program FRANC2D/L [6] using the J-integral approach by Dodds and Vargas [7]. The influence of K_I and K_{II} on fatigue crack growth was based on the maximum tangential stress criterion by Erdogan and Sih [8]. It predicts that the fatigue crack propagation path is perpendicular to the maximum principal stress and the crack grows under the Mode I. The local asymptotic LEFM crack front fields can be described as [9]:

$$\sigma_{rr} = \frac{1}{\sqrt{2\pi r}} \cos\frac{\theta}{2}\left[K_I \left(1+\sin^2\frac{\theta}{2}\right) + \frac{3}{2} K_{II} \sin\theta - 2K_{II} \tan\frac{\theta}{2}\right] + \frac{T}{2}(1+\cos 2\theta), \quad (1)$$

$$\sigma_{\theta\theta} = \frac{1}{\sqrt{2\pi r}} \cos\frac{\theta}{2}\left[K_I \cos^2 \frac{\theta}{2} - \frac{3}{2} K_{II} \sin\theta \right] + \frac{T}{2}(1-\cos 2\theta), \quad (2)$$

$$\sigma_{r\theta} = \frac{1}{2\sqrt{2\pi r}} \cos\frac{\theta}{2}\left[K_I \sin\theta + K_{II}(3\cos\theta - 1)\right] - \frac{T}{2}\sin 2\theta\,, \quad (3)$$

where σ_{rr}, $\sigma_{\theta\theta}$ and $\sigma_{r\theta}$ are the stress components from a distance r and angle θ from the crack tip in the cylindrical-polar coordinate system. The *T*-stress is a constant component of the stress field and acting parallel to the crack tip. With using first-order kinking theory, differentiating the first term in Equation (2) with respect to θ and denoting $\theta = \Delta\theta_c$, the crack growth direction perpendicular to the maximum principal stress can be expressed as [9]:

$$\Delta\theta_c = 2\tan^{-1}\left(\frac{1-\sqrt{1+8(K_{II}/K_I)^2}}{4(K_{II}/K_I)} \right). \quad (4)$$

Mixed-mode interaction can be considered by neglecting the second term from the Equation (2), denoting $\theta = \Delta\theta_c$, multiplying both sides with $\sqrt{2\pi r}$ and denoting the left side as $\Delta K_{I_{eq}}$, i.e., the tangential stress $\sigma_{\theta\theta}$ in the Mode I is put equal to the $\sigma_{\theta\theta}$ in the Mode I and Mode II combination. Then, the equivalent SIF will be:

$$\Delta K_{I_{eq}} = \left(K_I \cos^2 \frac{\Delta\theta_c}{2} - \frac{3}{2} K_{II} \sin\Delta\theta_c \right) \cos\frac{\Delta\theta_c}{2}\,. \quad (5)$$

When the loading is a pure shear Mode II with a crack kink angle of -70.5°, $\Delta K_{I_{eq}} = 1.15 K_{II}$. The crack growth direction will change if the initial crack direction does not satisfy the propagation direction in the Mode I. The ΔK_{Ieq} will be approximately equal to K_I for the following crack propagation steps, if the crack growth increment is small enough [10].

Fatigue life calculation

For the fatigue life calculation, the Paris–Erdogan relationship [11] was used. It has the following form:

$$\frac{da}{dN} = C(\Delta K)^m\,, \quad (6)$$

where a is the crack length, N is the number of cycles, C is a material constant, ΔK is the opening mode SIF range and m is also a material constant and the phase *II* slope on log-log plot. Stress ratios R >0 can be assessed by a form of the crack propagation equation proposed by Forman [12]:

$$\frac{da}{dN} = \frac{C(\Delta K)^m}{1-R}. \tag{7}$$

The N can be solved with separating the variables and integrating:

$$N_{if} = \int_{a_i}^{a_f} \frac{(1-R)da}{C(\Delta K)^m}. \tag{8}$$

For the material constants, $C_{char} = 3.0 \cdot 10^{-13}$, $C_{mean} = 1.7 \cdot 10^{-13}$ and m = 3 (in $Nmm^{-3/2}$ and mm units) were used and they are recommended by International Institute of Welding (IIW) [13] for fatigue assessment of ferrite-pearlite steel welded joints in as-welded condition. C_{mean} is the mean crack growth rate coefficient and C_{char} is the characteristic crack growth coefficient corresponding to 95 % survival probability. The threshold ΔK_{th} value was not used in this study.

Fatigue analysis with fatigue crack growth simulator

Model generation

Fatigue crack growth simulations were executed with a typical desktop PC with Pentium microprocessor. With symmetry boundary conditions (BCs), only one-quarter of the structure had to be modeled. Weld throat and plate thickness were considered to have the constant values of A = 6.5 mm and T = 10 mm, Figure 2. For the material model, Young's modulus E = 210000 MPa and Poisson's ratio ν = 0.3 was used. The heat-affected zone was not considered.

For the mesh, isoparametric eight noded elements with quadratic shape functions were used and the singularity problem in the crack tip was solved by moving the side nodes to the quarter-point positions [14]. A typical model can be seen on Figure 3. The dimensions of the models were altered to study the parametric relationship on the fatigue strength. For flank angles β = 30°, 45°, 60°, toe radius r/T ratios 0.05, 0.1, 0.2, 0.4, 1 and cold lap a/T ratios 0, 0.01, 0.02, 0.04, 0.08, 0.16 were used.

The crack growth simulation started from an initial edge crack direction perpendicular to the global x-axis at end of the cold lap. For the initial crack length, 0.05 mm was used. It was then increased with increments of 0.01, 0.02, 0.05, 5 x 0.1, 5 x 0.2, and 5 x 0.5. Those models that did not have a cold lap (a/T ratio was 0), the initial crack length was 0.05 mm and the crack began to grow at the weld toe. The final crack size, Figure 4, developed to the length with magnitude of 4.085 mm, which corresponded to 81.7 % of the double symmetrical models plate thickness.

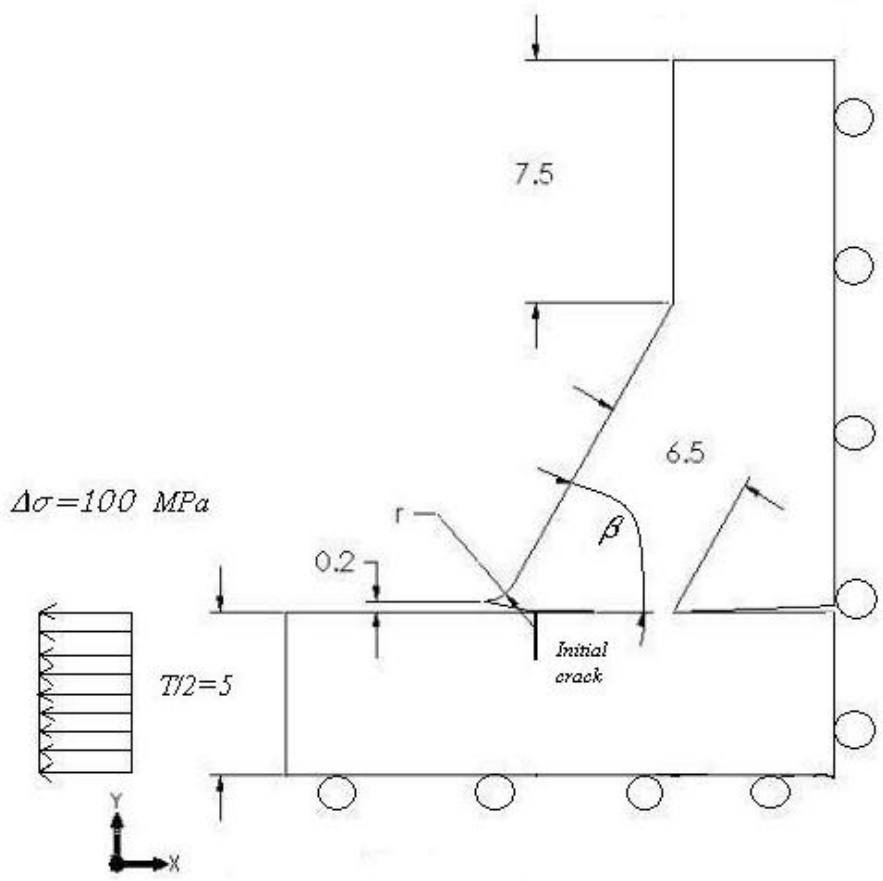

Figure 2. A double symmetric model with boundary conditions and loading.

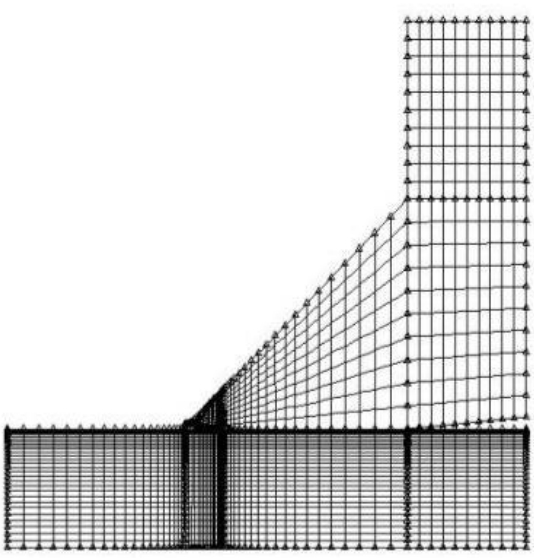

Figure 3. Typical mesh size.

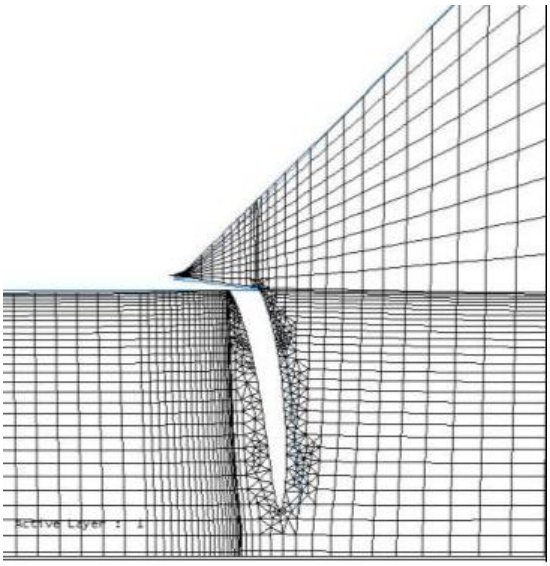

Figure 4. Final deformed mesh.

Fatigue strength calculation

Fatigue strength of a welded joint is characterized by a fatigue class, FAT [13], which identifies the stress range corresponding to $2 \cdot 10^6$ cycles to failure with a 95 % survival probability calculated from a mean value of a two-sided 75 % confidence level. In this study, The Paris-Erdogan relationship, Equation (6) and Equation (8) was used with equivalent Mode I values of the SIF range to obtain the cycles to failure. To convert the cycles to failure to a characteristic fatigue class were carried out as follows [15]:

$$FAT = \Delta\sigma_{ref} \sqrt[3]{\frac{N_{ref}}{2 \cdot 10^6}}, \tag{9}$$

where $\Delta\sigma_{ref}$ was the adapted tensile load of 100 MPa and N_{ref} was the predicted fatigue life of the given model. To compare the results from the crack growth simulation with 50 % survival probability to the experimental fatigue test results, a conversion was made:

$$FAT_{mean} = \sqrt[3]{\frac{C_{char}}{C_{mean}}} \cdot FAT \approx 1.208 \cdot FAT, \tag{10}$$

where FAT_{mean} is the mean fatigue strength at $2 \cdot 10^6$ cycles.

Results

Non-linear regression analysis

The results from the crack growth simulation for each model are represented in Appendices. For the initial crack, the stress intensity factor ranges for K_I and K_{II} along with the crack kink angles $\Delta\theta_c$ were obtained from the simulator. Then, the equivalent stress intensity factors ΔK_{Iieq}were calculated separately. The FAT, relative toe radius r/T, relative cold lap size a/T and flank angle β were curve-fitted with non-linear regression analysis [16]. The parametric Equation (11) along with the adjunction functions, Equations (12, 13 and 14), are presented below. The parameters for the parametric equation and adjunction functions are presented in the Table 1. Furthermore, the average deviation and the maximum deviation from the predicted FAT of the parametric Equation (11) are presented lastly.

$$FAT\left(\frac{a}{T}, \frac{r}{T}, \beta\right) = \frac{m_i}{f_{1i}\left(\frac{r}{T}, \beta\right) + f_{2i}\left(\frac{r}{T}, \beta\right) \cdot \left(\frac{a}{T}\right)^{f_{3i}\left(\frac{r}{T}, \beta\right)} + p_i \cdot \left(\frac{r}{T}\right) + q_i \cdot \left(\frac{r}{T}\right)^2}, \tag{11}$$

where

$$f_{1i}\left(\frac{r}{T},\beta\right)=\frac{1}{a_i+b_i\cdot\left(\frac{r}{T}\right)^{c_i}}, \tag{12}$$

$$f_{2i}\left(\frac{r}{T},\beta\right)=d_i\cdot g_i^{\left(\frac{r}{T}\right)}\cdot\left(\frac{r}{T}\right)^{h_i}, \tag{13}$$

$$f_{3i}\left(\frac{r}{T},\beta\right)=k_i\cdot\left(\frac{r}{T}\right)^{l_i}, \tag{14}$$

i = 1, 2, 3.

Table 1. Parameters for the Equations (11), (12), (13) and (14)

i	1	2	3
β	30^o	45^o	60^o
a_i	-0,2436	1,936	1,985
b_i	4,551	2,527	2,408
c_i	0,08605	1,070	0,9115
d_i	0,4131	2,083	1,189
g_i	0,3871	0,09862	0,1687
h_i	0,5511	1,309	1,130
k_i	0,4274	0,3803	0,3629
l_i	0,07039	0,1524	0,1473
m_i	24,34	36,24	34,92
p_i	-0,02286	0,009579	0,08232
q_i	0,01236	0,09913	0,008154
Average deviation	0.9004	0.5470	0.7182
Max. deviation	4.587	1.867	1.973

Data plots

The results from the crack growth simulation (Appendices: Table 1, 2 and 3) are represented as the 3D surface plots below to each flank angle. Lastly, all the 3D flank angle plots are represented together along with the corresponding IIW fatigue class 80 [13].

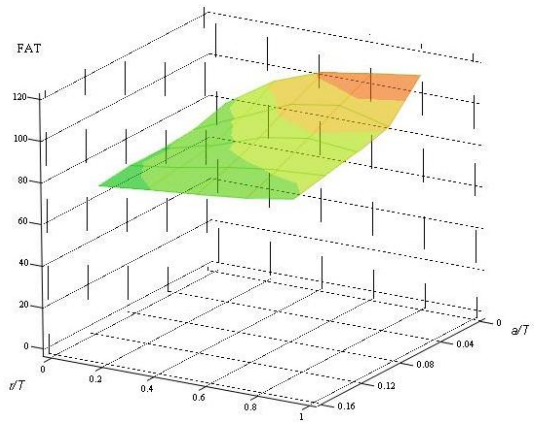

Figure 5. Flank angles of 30 degrees.

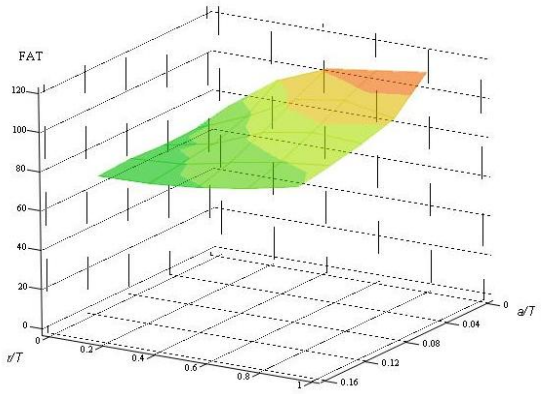

Figure 6**.** Flank angles of 45 degrees.

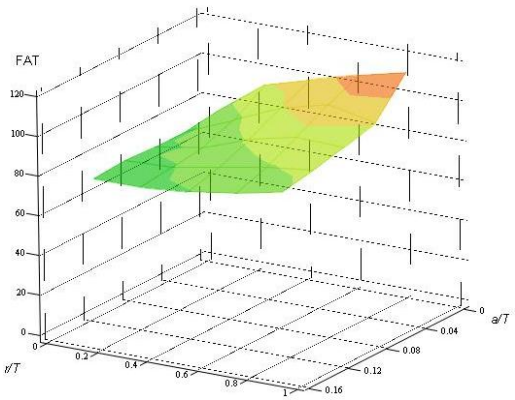

Figure 7. Flank angles of 60 degrees.

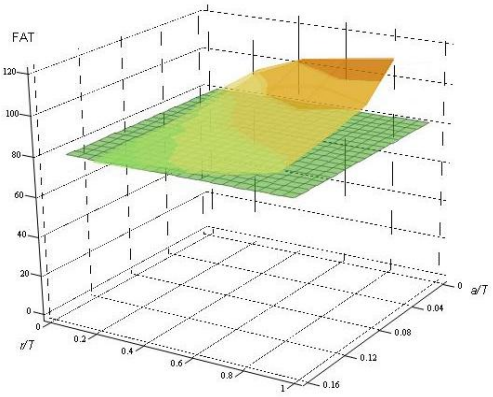

Figure 8. Results from the study plotted jointly with the IIW recommendation (FAT 80) to non-load-carrying fillet welded cruciform joints

Comparison to test results

The FAT results from the FEA were compared with the available test results of non-load-carrying cruciform joints from three different sources; Martinsson [1] examined specimens with the yield strength of 380 MPa, thickness of 12 mm and welded with tandem arc MAG; Barsoum [17] examined as well also specimens with 12 mm of thickness, but they were welded with hybrid Nd:YAG-laser/MAG and MAG; Sehadri [18], investigated at the Lappeenranta University of Technology (LUT), specimens with 6 mm of thickness and with two different yield strength, 355 MPa and 650 MPa. Sehadri classified weld defects from the test specimens and all test specimens were micrographed, Figure 9. Martinsson and Barsoum used $R = 0$ for the stress ratio while LUT [18] used varying stress ratio with $R = 0.10$ to $R = 0.66$. The specimens and batches are listed in the Table 2.

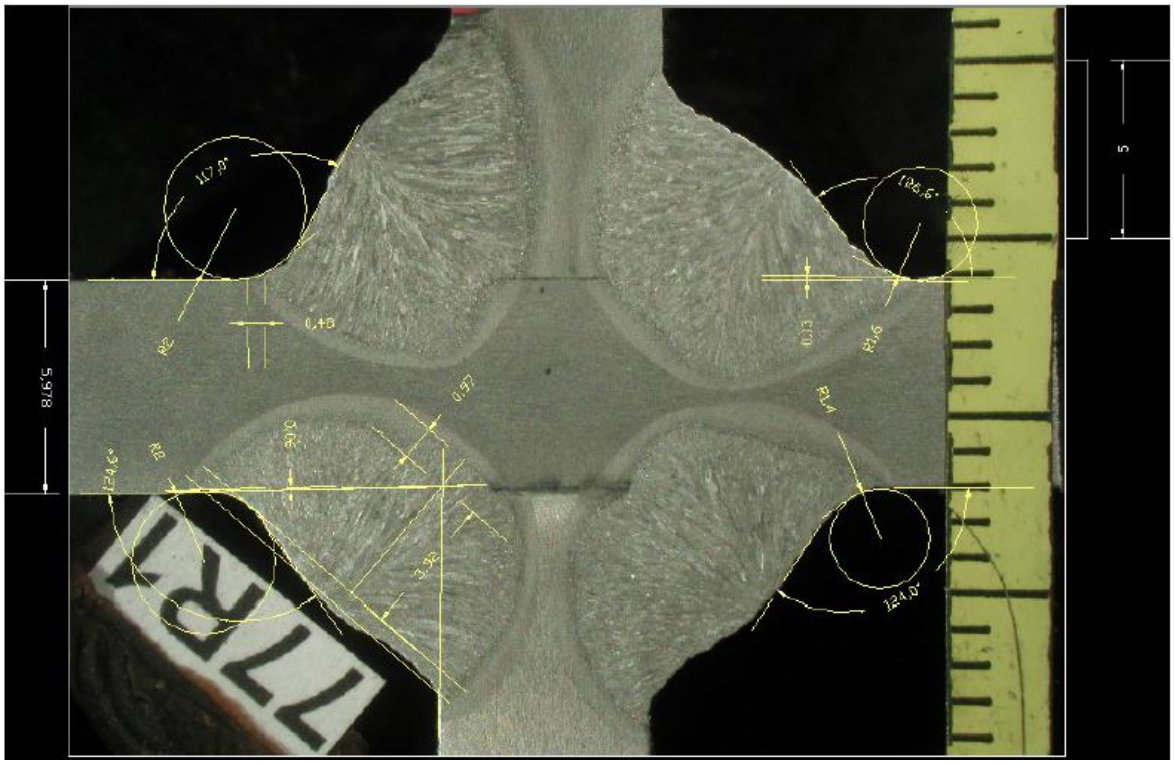

Figure 9**.** Micrograph from a test specimen [18].

Only those specimens that were in the range of this parametric study, i.e. r/T within 0.05 – 1, a/T within 0 - 0.16 and β bound to 30^{o}- 60^{o}, were selected to the comparison; e.g. from Martinsson and Sehadri, only the above-mentioned geometrical constraints satisfying individual specimens were selected. However, because of the absence of a more detailed description, four batches were selected from Barsoum and FATexp were estimated with the average value of all specimens in the certain batch. Values for the flank angle β were estimated from the LUT's test specimens by subtracting the measured toe angles from 180 degrees [18].

Comparison was made with the following way: firstly, the geometrical dimensions from the specimens and batches were converted to the ratios with the respect of plate thickness, Table 3. Secondly, a prediction from the parametric Equation (11) was calculated with a given geometrical ratio and converted to mean fatigue strength with the Equation (10). Thirdly, if the flank angles on the specimens were not occurred to be 30, 45 or 60 degrees, the corresponding mean fatigue strength with a given flank angle was linearly interpolated [19]. Finally, the average, maximum and standard deviation were calculated from the comparison.

Table 2.Test specimens.

Specimen / Batch	Welding method	T [mm]	σ_y [MPa]	Remarks
C1 [1]	MAG	12	380	Tandem arc
C2	MAG	12	380	
C3	MAG	12	380	
C5	MAG	12	380	
C6	MAG	12	380	
D2	MAG	12	380	
D5	MAG	12	380	
L [17]	YAG-laser/MAG	12	360	
C	MAG	12	360	Tandem arc, solid wire
E	MAG	12	360	Flux cored wire
F	MAG	12	360	Tandem wire, flux cored
A1	MAG	12	390	Manual welding
A2	MAG	12	390	Robotic welding
B	MAG	12	490	Manual welding
01 [18]	MAG	6	355	
04	MAG	6	355	
35	MAG	6	650	
77	MAG	6	650	

Table 3. Comparison to test results of non-load-carrying cruciform joints

Specimen/ Batch	$\frac{r}{T}$	$\frac{a}{T}$	β [deg]	FAT_{exp} [MPa]	FAT_{cal} [MPa]	FAT_{mean} 30 deg	FAT_{mean} 45 deg	FAT_{mean} 60 deg	SCF Mean/ Std.dev.
C1 [1]	0.083	0.033	53	94	88	92	87	88	3
C2	0.083	0.025	48	126	87	93	87	88	2.2
C3	0.250	0.025	40	103	96	100	94	94	2.6
C5	0.083	0.025	60	98	88			88	3
C6	0.166	0.025	50	113	90	97	90	91	2.6
D2	0.083	0.025	60	98	88			88	2.6
D5	0.660	0.025	60	100	106			106	3
L [17]	0.160	0.050	30	113	94				2.7 / 0.5
C	0.200	0.050	30	106	95				2.7 / 0.3
E	0.092	<0.003	30	136	98	98			2.6 / 0.6
F	0.283	<0.016	30	121	103	103			1.8 / 0.1
A1	0.083	0.008	50.6	98	104		105	103	3.4 / 1.2
A2	0.225	0.010	49.5	110	95		95	95	2.5 / 0.5
B	0.083	0.008	45	106	88				3.2 / 1.0
01[18]	0.075	0.026	48	108	87	93	87	88	2.87
04	0.075	0.078	53	100	86	89	86	87	2.95
35	0.260	0.051	46	104	91	96	91	92	1.96
77	0.167	0.080	50	85	87	92	87	88	2.3
Avg.dev. %					-12.77				
Max.dev. %					-30.95				
Std.dev. %					9.79				

FAT_{exp} is the experimental fatigue strength at $2 \cdot 10^6$ cycles and FAT_{cal} is the mean fatigue strength at $2 \cdot 10^6$ calculated from the Equations (10) and (11). To examine the accordance and conformity of the FAT_{exp} and FAT_{cal}, they were plotted with an ideal reference line along with + 20 % and – 20 % lines, Figure 10. If the correspondence would be perfect, the points would subside to the reference line in the middle.

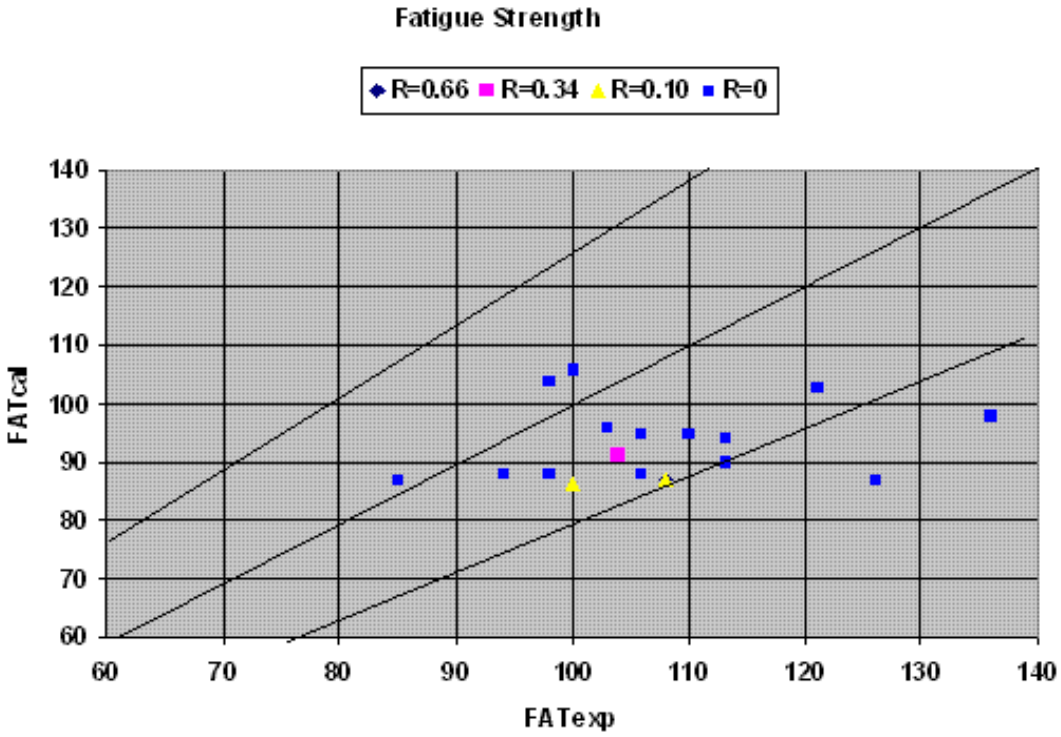

Figure 10. Comparison of fatigue strength with specimens and FEA

The Figure 10 illustrates that there was scatter between the test results and FEA. Moreover, when the points seemed to settle under the reference line, it meant that, the FEA allows more conservative fatigue strength and life predictions than what was perceived from the experimental endurance test results with real specimens.

The trend with the comparisons, Figure 10, seemed to be that the FEA allocates more conservative fatigue strength and life predictions in plurality of the cases than what was observed experimentally from the real test specimens on the endurance tests.

Discussions

The objective of this work was to study the influence of cold laps on the non-load-carrying fillet welded cruciform joints fatigue strength in as-welded condition under cyclic tensile loading. The fatigue analysis data from the crack growth simulator indicated that there was a significant difference in FAT for a given flank angle when the local geometry was varied; e.g. with the 45° models, the FAT with 95 % survival probability increased from 70.4 MPa to 109.1 MPa by smoothing the toe radius and eliminating the cold lap. Comparable values from the models with 30° and 60° flank angles were 71.1 MPa to 109.8 MPa and 71.4 MPa to 110.5 MPa. When the *r/T* ratio was increased from 0.05 to 1.0 and within the *a/T* ratio of 0.16 to models with 30°, 45° and 60° flank angles,

it produced a difference of 11.3 MPa, 12 MPa and 10.7 MPa in the FAT. With that kind of difference, the theoretical FAT could be raised by one fatigue class [13].

Cold laps also proved to have a serious effect on the fatigue strength; e.g. with the 60^o models with 1.0 *r/T* ratio, the FAT decreased from 110.5 MPa to 82.1 MPa, creating a difference of 28.4 MPa, when the *a/T* ratio was increased from 0 to 0.16. With the 30^o and 45^o flank angles equivalent prolepses were 27.4 MPa and 26.7 MPa. The difference with that kind of magnitude inflicts proceeding to the two step higher fatigue class. However, with a sharper toe radius, the difference did not mount as much and the influence of the *r/T* ratio, i.e. local notch, on the fatigue strength is self-evident. Also, compared to the models without a cold lap, the FAT decreased more with a smoother toe radius. This seemed to be in correspondence with numerous studies [1, 4, 17], that with high SCF (stress concentration factor) values, cold laps effect on the fatigue strength will become almost imperceptible and a sharp toe radius, i.e. small *r/T* ratio, is the primary contributor to the high stress concentrations, thus the most influential factor on the fatigue strength.

Variation on the flank angle seemed to have only minimal effects on the fatigue strength with examined flank angle range and that can be observed from Figures 5, 6 and 7. The 3D surface plots from the results seemed to be almost identical. However, the fatigue strength is usually greater with a gently sloping flank angle, Table 1, and it is documented that the effect of flank angle on the fatigue strength is minimal when the *r/T* ratio is large and increases when the toe radius decreases [15]. This study supports those conclusions.

When comparing the FEA results to the test results, the correlation seemed to be satisfying and occasionally scattering; e.g. when compared to the batches and specimens that were in the examined range with their geometrical parameters, the largest deviation was ≈ - 31 % with specimen C2, Table 6, from Martinsson and the smallest deviation of 2 % with specimen 77 from LUT, while the mean of the specimens was ≈-12 %. Three of the largest deviations came from the specimens and batches with thickness of 6 - 12 mm, *r/T* ratios of 0.083, 0.092 and 0.075, *a/T* ratios of 0.025, 0.003 and 0.026. The flank angles were 48^o, 30^o and 48^o, the yield strength varied from 355 MPa to 380 MPa and the welding processes were similar. They all had SCFs from 2.2 to 2.87. It was notable that the correlation between FAT_{exp} and FAT_{cal} was more unsubstantial with 12 mm specimens when they all had a small SCF, while with the LUT's specimens with 6 mm of thickness, the correlation was better the more lower the SCF went. Best correlation came from the 50^o and 60^o flank angles. Only three specimens proved to last less than the corresponding FAT_{cal} and that can be observed on Figure 10.

The reason of the difference between FEA and test results could be explained with the nature of LEFM and FEM; it is well documented [15], that the predictions with 2D LEFM in plain strain will be more conservative than the experimental test data from the real case, because the crack will grow semi-elliptically in the real structure [20]. Furthermore, the compressive residual stresses in weld toe on Batch E [17] and the non-existent cold laps, will affect definitely on the divergence between the conservative planar LEFM analysis and the experimental tests. Moreover, the influence of throat thickness variation on the fatigue strength has not been considered in this paper and the study was carried out with constant throat thickness of 6.5 mm. However, there is evidence [21] that the variation of throat thickness will only have small effect on the fatigue strength. It can also be observed from the Figure 9, that the determination of the flank angle β from the real specimens for FEA is rather difficult because the welds usually have a certain convexity. Furthermore, the LEFM approach was conducted with using $C_{char} = 3.0 \cdot 10^{-13}$ [13] as the material parameter, but IIW (2004) [22] and British Stan-

dard 7910: 1999 [23] have recommended slightly higher values with C_{char}= 5.0·10^{-13} and C_{char}= 5.21·10^{-13}, which reduces the predicted FAT with 95 % survival probability by 15.6 % and 16.8 %. This leads into more conservative fatigue strength predictions.

Finally, a conclusion could be made that the parametric Equation (11) predicts effectively credible and slightly conservative FAT values that can be used on fatigue analysis and design. The study was made with steel as the material, but the parametric equation can be also used to aluminium, when the FAT is reduced to one-third from the original value [20]. LEFM works most accurately to welds with lower quality than welds with smooth toe radius and without any significant defects due to negligence of crack initiation period, which's proportion of total fatigue life increases with high quality welds [20, 24].

Conclusions

The objective of this work was to study the influence of cold laps on the fatigue strength of non-load-carrying fillet welded cruciform joints under cyclic tensile loading. The assumption of as-welded condition made the fatigue crack initiation period to be considered non-existent. LEFM in plain strain was used for fatigue analysis with several FE models and different weld geometry variations. The ratio of cold lap size and toe radius to the plate thickness and the flank angle were systematically altered and analyzed and the parametric relationships between those variables were formulated with the respect of FAT with 95% survival probability and curve-fitted to a parametric Equation (11). Steel was used as the material and the FAT predictions will cover also aluminium when the FAT value is reduced to one-third. The FAT predictions from the parametric equation were converted to mean fatigue strength, FAT_{mean}, and compared to numerous test results with different investigations of non-load-carrying fillet welded cruciform joints. Based on these proceedings, the following conclusions can be made:

1) Cold laps effect significantly on the fatigue strength.

2) With a small toe radius, cold laps will not effect on the fatigue strength nearly as much as with a large toe radius.

3) Variation in the flank angle from 30 to 60 degrees will not produce a considerable fluctuation on the fatigue strength.

4) The predictions from the analytical model are corresponding with the test results from similar structure details and weld defects.

5) Cold laps substantial effect on the fatigue strength is evident and should be consid ered critically in designing, fabrication and quality inspecting stages.

6) LEFM in plane strain works well for this kind of problem and allocates creditable predictions that are most accurate on welds with lower quality due to non-existent crack initiation period.

Acknowledgements

This work was conducted in the Department of Mechanical Engineering at the Lappeenranta University of Technology as the part of the "LAATU" weld quality project, funded by Finnish industry and the National Technology Agency of Finland. Acknowledgements go to Professor Gary Marquis and Dr. Timo Nykänen, who supervised this study and to Dr. Timo Björk, who was the Project Coordinator.

References

[1] Martinsson, J. *Fatigue Strength of Welded Cruciform Joints with Cold Laps. Design and Analysis of Welded High Strength Steel Structures.* 2002. EMAS ltd. ISBN 1 901537 34 X.

[2] NDT Resource center. [On-Line]. Retrieved January 3rd 2007 from: http://www.ndt-ed.org/.

[3] Lopez Martinez, L. and Korsgen, S. *Characterization of Welded Defect Distribution and Weld Geometry in Welded Fatigue Test Specimens. Fatigue Under Spectrum Loading an in Corrosive Environments.* 1993. EMAS ltd. Warley, UK.

[4] Samuelsson, J. *Cold Laps and Weld Quality Acceptance Limits. Design and Analysis of Welded High Strength Steel Structures.* 2002. EMAS ltd. ISBN 1 901537 34 X.

[5] Martinsson, J. *Fatigue Assessment of Complex Welded Structures.* Doctoral Thesis. 2005. ISBN 91-2783-968-6. [On-Line]. Retrieved December 25th 2006 from: http://www.divaportal.org/diva/getDocument?urn_nbn_se_kth_diva_166-2_fulltext.pdf

[6] James M. and Swenson D. FRANC2D/L: A Crack Propagation Simulator for Plane Structures. Available from: http://www.mne.ksu.edu/~franc2d/.

[7] Dodds RH and Vargas PM, Numerical evaluation of domain and contour integral for nonlinear fracture mechanics: formulation and implementation aspects. Report from University of Illinois at Urbana-Champaign, Dept. of Civil Engineering, 1988.

[8] Erdogan F. and Sih GC. ASME J Basic Engng 1963; 85: 519-527.

[9] Ingraffea, A., Wawrzynek, P. *Finite Element Methods for Linear Elastic Fracture Mechanics.*Chapter 3.1 in Comprehensive Structural Integrity. 2003. Elsevier Science Ltd., Oxford, England.[On-Line]. Retrieved November 1st 2008 from:http://www.cfg.cornell.edu/education/education.htm.

[10] Nykänen, Timo. *Fatigue crack growth simulations in laser welded lap joints*. IIW-Document XIII-1707-98.

[11] Paris, P.C and Erdogan, F. A critical analysis of crack propagation law, *Trans ASME, J Basic Eng*, 1963, 85, 528-539.

[12] Forman, R. G., Kearney, V.E. and Engle, R.M. Numerical analysis of crack propagation in cyclic loaded structures, *Trans ASME, J Basic Eng*, 1967, 89, 459.

[13] Hoppacher, A. Fatigue Design of Welded Joints and Components, Recommendations of IIW Joint Working Group XIII-XV, doc. XIII-1539-96/XV-845-96, Abington Publishing, 1996.

[14] Bathe, K-J. *Finite Element Procedures,* Prentice-Hall, Inc. A Simon & Schuster Company, Eaglewood Cliffs, New Jersey 07632, 1996.

[15] Nykänen, T., Marquis, G. and Björk, T. Fatigue analysis of non-load-carrying fillet welded cruciform joints. *Engineering Fracture Mechanics,* Volume 74, Issue 3, pp. 399-415, February 2007.
[16] Sherrod PH. NLREG. Nonlinear Regression Analysis Program. Available from: http://www.nlreg.com/.
[17] Barsoum, Z. Fatigue Strength of Cruciform Joints Welded with Different Welding Processes. International Symposium on Integrated Design and Manufacturing of Welded Structures. March 13-14, 2007, Eskilstuna, Sweden.
[18] Sehadri, A. Statistical Variation of Weld Profiles and Their Expected Influence on Fatigue Strength. Master's Thesis. 2006. Lappeenranta University of Technology.
[19] Hyams, D. CurveExpert 1.3. A comprehensive curve fitting system for Windows. Availablefrom: http://www.ebicom.net/~dhyams/cmain.htm.
[20] Radaj, D. and Sonsino, C-M. *Fatigue assessment of welded joints by local approaches*, Woodhead Publishing Ltd, 1998.
[21] Nykänen, T., Marquis, G., Björk, T. Approximative master curve for fatigue assessment of cruciform joints with non-load-carrying welds. Finnish Welding Society Design Forum 7 – 8.6.2007, Lahti.
[22] Hobbacher, A. Recommendations for Fatigue Design of Welded Joints and Components. IIWDocument XIII-1965-03/XV-1127-03. Update July 2004.
[23] Guide on methods for assessing the acceptability of flaws in metallic structures, British Standard BS 7910:1999, 1999.
[24] Björk, T., Marquis, G., Quality Assessment of Welds for Fatigue Loaded Structures. International Symposium on Integrated Design and Manufacturing of Welded Structures. March 13-14, 2007, Eskilstuna, Sweden.

Mikko Heiskanen
Konecranes Heavy Lifting Corporation
P.O. Box 662
FIN-05801 Hyvinkää
FINLAND
e-mail: Mikko.Heiskanen@konecranes.com

Appendix Results from fracture mechanics analysis

Table A1. Results for the models with flank angle of 30 degrees

Model	β	*r/T*	*a/T*	*FAT*	K_I	K_{II}	$\Delta\theta_c$	$\Delta K_{I_{ieq}}$
30-1	30	0,05	0,0	78,8	87,2	-6,7	8,7	87,9
30-2	30	0,05	0,01	76,1	91,1	-28,9	30,3	103,0
30-3	30	0,05	0,02	75,4	91,1	-31,2	31,9	104,8
30-4	30	0,05	0,04	74,2	96,1	-29,2	29,4	108,1
30-5	30	0,05	0,08	72,7	103,9	-35,4	31,8	119,3
30-6	30	0,05	0,16	71,1	116,2	-42,5	33,3	135,7
30-7	30	0,1	0,0	88,7	72,5	-7,7	11,9	73,7
30-8	30	0,1	0,01	78,8	68,1	-15,4	23,4	73,0
30-9	30	0,1	0,02	76,9	69,1	-20,1	28,4	76,8
30–10	30	0,1	0,04	76,1	75,4	-23,1	29,5	84,7
30–11	30	0,1	0,08	73,9	88,7	-18,8	22,1	94,2
30-12	30	0,1	0,16	72,1	108,2	-38,6	32,8	125,6
30-13	30	0,2	0,0	88,7	67,9	-1,9	3,3	68,0
30-14	30	0,2	0,01	88,7	47,4	-15,8	38,8	59,5
30-15	30	0,2	0,02	81,6	53,5	-23.4	37,3	65,7
30-16	30	0,2	0,04	79,3	61,2	-26,8	37,3	75,2
30-17	30	0,2	0,08	75,7	72,2	-35,9	40,1	92,5
30-18	30	0,2	0,16	73,1	77,1	-39,4	40,6	99,8
30-19	30	0,4	0,0	100	57,1	-4,5	9,1	57,6
30-20	30	0,4	0,01	89,8	34,5	-15,8	38,3	43,1
30-21	30	0,4	0,02	85,4	47,6	-22,4	38,9	59,8
30-22	30	0,4	0,04	82,4	52,4	-18,2	32,2	60,5
30-23	30	0,4	0,08	79,8	51,8	-28,8	42,4	69,2
30-24	30	0,4	0,16	74,5	62,7	-35,4	42,8	84,2
30-25	30	1,0	0,0	109,8	50,2	-2,1	4,7	50,4
30-26	30	1,0	0,01	100,6	36,7	-16,1	37,3	45,1
30-27	30	1,0	0,02	95,1	53,4	-14,4	26,9	58,7
30-28	30	1,0	0,04	93,2	55,9	-13,6	24,8	60,4
30-29	30	1,0	0,08	88,7	63,6	-14,5	23,5	68,2
30-30	30	1,0	0,16	82,4	68,7	-21,7	30,2	77,6

Table A2**.** Results for the models with flank angle of 45 degrees.

Model	β	*r/T*	*a/T*	*FAT*	K_I	K_{II}	$\Delta\theta_c$	$\Delta K_{I_{ieq}}$
45-1	45	0,05	0,0	74,2	97,6	-9,3	10,7	98,9
45-2	45	0,05	0,01	72,4	101,2	-32,9	30,8	115,1
45-3	45	0,05	0,02	71,4	111,3	-30,1	26,9	122,2
45-4	45	0,05	0,04	71,1	106,1	-35,6	31,5	121,6
45-5	45	0,05	0,08	70,4	108,3	-35,1	30,7	123,3
45-6	45	0,05	0,16	70,4	125,3	-42,0	31,5	143,3
45-7	45	0,1	0,0	78,2	82,6	-4,9	6,8	83,1
45-8	45	0,1	0,01	74,2	95,6	-30,1	30,1	107,9
45-9	45	0,1	0,02	73,1	96,9	-30,8	30,3	109,7
45-10	45	0,1	0,04	71,4	105,1	-27,1	25,9	114,5
45-11	45	0,1	0,08	70,8	106,7	-32,7	29,5	119,8
45-12	45	0,1	0,16	70,8	109,0	-40,7	33,8	128,0
45-13	45	0,2	0,0	84,3	71,1	-2,6	4,2	71,2
45-14	45	0,2	0,01	78,5	63,7	-27,4	36,9	77,8
45-15	45	0,2	0,02	76,6	82,2	-28,8	32,4	95,1

45-16	45	0,2	0,04	74,6	93,9	-31,4	31,4	107,4
45-17	45	0,2	0,08	72,1	95,9	-35,5	33,6	112,4
45-18	45	0,2	0,16	71,1	107,2	-34,6	30,6	121,6
45-19	45	0,4	0,0	99,3	55,9	-4,2	8,5	56,4
45-20	45	0,4	0,01	86,1	54,3	-21,2	34,8	64,5
45-21	45	0,4	0,02	82,9	67,5	-16,8	25,3	73,2
45-22	45	0,4	0,04	80,9	67,5	-19,7	28,5	75,1
45-23	45	0,4	0,08	76,1	84,4	-25,3	29,1	94,4
45-24	45	0,4	0,16	71,7	98,8	-37,6	34,2	116,6
45-25	45	1,0	0,0	109.1	50.5	-1.4	3.3	50,6
45-26	45	1,0	0,01	96,5	49,0	-17,6	33,0	57,0
45-27	45	1,0	0,02	96,1	49,3	-16,4	31,3	56,3
45-28	45	1,0	0,04	93,5	53,2	-9,9	19,8	55,9
45-29	45	1,0	0,08	88,7	61,1	-15,2	25,	66,3
45-30	45	1,0	0,16	82,4	65,8	-22,6	32,0	75,8

Table A3. Results for the models with flank angle of 60 degrees

Model	β	*r/T*	*a/T*	*FAT*	K_I	K_{II}	$\Delta\theta_c$	$\Delta K_{I_{ieq}}$
60-1	60	0,05	0,0	73,6	97,7	-7,7	8,9	98,6
60-2	60	0,05	0,01	72,1	107,5	-35,6	31,2	122,7
60-3	60	0,05	0,02	71,4	111,9	-35,8	30,4	126,7
60-4	60	0,05	0,04	71,4	120,9	-36,5	29,2	135,4
60-5	60	0,05	0,08	71,4	121,3	-37,5	27,3	136,3
60-6	60	0,05	0,16	71,4	125,2	-37,2	28,9	140,0
60-7	60	0,1	0,0	77,7	83,9	-4,4	6,0	84,3
60-8	60	0,1	0,01	74,8	66,8	-33,3	40,1	85,6
60-9	60	0,1	0,02	73,6	77,8	-37,5	39,4	98,5
60-10	60	0,1	0,04	72,4	85,3	-37,0	37,1	104,5
60-11	60	0,1	0,08	71,7	95,6	-42,5	37,6	118,0
60-12	60	0,1	0,16	71,7	126,7	-35,4	27,6	139,9
60-13	60	0,2	0,0	87,0	69,2	-3,0	5,0	69,4
60-14	60	0,2	0,01	77,7	75,9	-20,4	26,7	83,3
60-15	60	0,2	0,02	76,0	87,3	-22,6	26,0	95,3
60-16	60	0,2	0,04	74,5	80,2	-33,0	35,9	96,7
60-17	60	0,2	0,08	72,4	85,5	-46,6	42,0	113,3
60-18	60	0,2	0,16	71,7	112,9	-25,6	23,4	120,9
60-19	60	0,4	0,0	94,3	59,3	-1,9	3,7	59,4
60-20	60	0,4	0,01	86,1	61,6	-15,1	24,9	66,7
60-21	60	0,4	0,02	82,9	68,5	-17,7	26,0	74,7
60-22	60	0,4	0,04	80,4	75,0	-19,8	26,4	82,1
60-23	60	0,4	0,08	76,0	91,1	-23,5	25,9	99,3
60-24	60	0,4	0,16	72,1	87,8	-34,0	34,6	104,1
60-25	60	1,0	0,0	110,5	49,1	-0,6	1,4	49,2
60-26	60	1,0	0,01	96,1	45,1	-16,6	33,6	52,8
60-27	60	1,0	0,02	95,0	51,6	-9,3	19,3	54,0
60-28	60	1,0	0,04	92,8	56,7	-11,7	21,7	60,1
60-28	60	1,0	0,08	88,7	64,7	-14,6	23,3	69,3
60-30	60	1,0	0,16	82,1	71,1	-23,2	30,9	80,9